

Methanol formation chemistry with revised reactions scheme

Valeriia Alekseevna Sokolova

Ural Federal University, 19 Mira street, Yekaterinburg, 620002, Russia; valeria.sokolova@urfu.ru
Engineering Research Institute “Ventspils International Radio Astronomy Centre” of Ventspils University College,
Inzenieru 101, Ventspils, LV-3601, Latvia

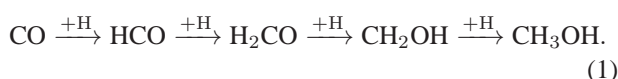
Received 2020 March 25; accepted 2020 June 10

Abstract The aim of the presented work is to analyze the impact of experimentally evaluated reactions of hydrogen abstraction on surfaces of interstellar grains on the chemical evolution of methanol and its precursors on grains and in the gas phase under conditions of a cold dark cloud and during the collapse of a translucent cloud into a dark cloud. Analysis of simulation results shows that those reactions are highly efficient destruction channels for HCO and H₂CO on grain surfaces, and significantly impact the abundances of almost all molecules participating in the formation of CH₃OH. Next, in models with those reactions, maximum abundances of methanol in gas and on grain surfaces decrease by more than 2–3 orders of magnitude in comparison to models without surface abstraction reactions of hydrogen. Finally, we study the impact of binding energies of CH₂OH and CH₃O radicals on methanol chemistry.

Key words: Astrochemistry — ISM: molecules — molecular processes — chemical networks — chemical modeling.

1 INTRODUCTION

Diverse molecular composition is one of the main properties of interstellar objects: it can include both simple and complex (more than six atoms) molecules (McGuire 2018). Complex organic molecules (COMs, molecules containing more than six atoms, including C and H) are species of special interest, because they are actively involved in prebiotic chemistry and are associated with the origin of life (Herbst & van Dishoeck 2009). Methanol (CH₃OH) is an important molecule for the formation of more complex organic compounds according to a number of laboratory and theoretical studies (Öberg et al. 2009; Murga et al. 2020; Rivilla et al. 2019; Kochina et al. 2013). It is assumed now (see e.g., Watanabe & Kouchi 2002; Fuchs et al. 2009; Linnartz et al. 2015) that methanol in the interstellar medium (ISM) forms on the surface of dust particles by hydrogenation of a carbon monoxide (CO) molecule, and then desorbs into the gas phase via thermal and non-thermal processes. Conventional hydrogenation that occurs on grain surfaces and leads from CO to CH₃OH (Tielens et al. 1991) is as follows



Recent laboratory experiments by Minissale et al. (2016) on atomic hydrogen exposure of carbon monoxide, formaldehyde and methanol thin films on cold surfaces revealed an unexpected desorption phenomenon. The analysis of experiments led the authors to the conclusion that the sequence of CO hydrogenation on grain surface must be explained. It was shown that it is necessary to include additional H₂-abstraction reactions (reverse reactions) for HCO and H₂CO into the scheme of surface methanol formation



Given the fundamental importance of methanol for interstellar chemistry of COMs, we decided to study the impact of these reactions on chemical evolution under different conditions of the ISM. This paper is organized as follows. Section 2 is dedicated to utilizing a method for computing molecular abundances and utilizing physical models. Section 3 describes the modeling results. Discussion of obtained modeling results is presented in Section 4.

2 METHODS

2.1 Calculating Molecular Abundances

We apply the MONACO code described in Vasyunin et al. (2017) to calculate abundances of species. It utilizes the rate equations method to numerically simulate the chemical evolution of the ISM, and includes treatment of chemistry in the gas phase and on grain surfaces under non-stationary conditions. This code calculates time-dependent fractional abundances of species with respect to the total number of hydrogen nuclei for each species in a given time interval. In our study we run two types of models: with and without reverse reactions for HCO and H₂CO from Minissale et al. (2016), where the reaction (3) has the activation barrier $E = 202$ K (Baulch et al. 2005).

In all models, we use the kinetic database utilized in Vasyunin et al. (2017), with binding energies $E_d(\text{CH}_2\text{OH}) = 5080$ K and $E_d(\text{CH}_3\text{O}) = 2540$ K (see table 2 in Wakelam et al. 2017). We denote the model without reverse reactions as Model I, and the model with reverse reactions as Model II.

2.2 Utilized Physical Models

In our analysis we utilized two physical models. The first model is a 0D model with time-dependent physical conditions that mimic the transition from a translucent cloud to a dark cloud. The second model represents a typical static dark molecular cloud.

The model of collapse was taken from Vasyunin & Herbst (2013a) and consists of two stages. At the first “cold” stage, the collapse proceeds in a free-fall regime and starts at a gas density $n_{\text{H}} = 3 \times 10^3 \text{ cm}^{-3}$ and visual extinction $A_V = 2^m$. The process continues until a density of 10^7 cm^{-3} is reached within 10^6 yr of evolution. During the cold stage, temperature linearly decreases from 20 to 10 K, and the gas temperature is assumed to be equal to the dust temperature. At the second “warm-up” stage, temperature is growing from 10 to 200 K with a square-law over 2×10^5 yr, which corresponds to models of the formation of intermediate-mass stars. Gas and dust temperatures are equal. Density and visual extinction remain constant. “High-metal” atomic initial composition corresponds to the values listed in column EA2 in table 1 from Wakelam & Herbst (2008).

The model of a cold dark cloud corresponds to the model described in Vasyunin & Herbst (2013b) and represents a typical cold dark molecular cloud: $T = 10$ K, proton density $n_{\text{H}} = 10^5 \text{ cm}^{-3}$, visual extinction $A_V = 10^m$ and “low-metal” initial composition (see Wakelam & Herbst 2008, column EA1 in table 1). Chemical evolution is simulated over a time span of 10^6 yr.

3 RESULTS

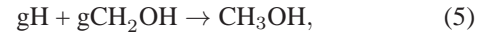
The results of simulations are displayed in Figures 1–3. Each plot represents time dependent abundances of methanol and some chemically related species.

3.1 Cold Cloud

In Figure 1, the abundances of methanol and chemically related species as a function of time in the gas phase and on the grain surface for the model of the cold dark cloud are presented.

In Model II, abundances of CH₃OH (both gaseous and on grain surface), gaseous CH₂OH, H₂CO, HCO and CO on grain surfaces show significant changes in comparison with Model I.

In Model I, the main methanol formation routes are through the following reactions on the grain surface followed by the efficient reactive desorption (here and after in formulas and in figures, all species on grain surfaces are marked with prefix ‘g’ while species without ‘g’-prefix are gaseous species)



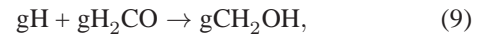
where the rate of reaction (4) is higher by a factor of three than in reaction (5). In Model II, reactions (4) and (5) become inefficient because of strong backward reactions in the nets of CH₃O and CH₂OH formation. Dissociative recombination of gaseous H₂COHOCH₂⁺ becomes the main route of gas phase methanol formation



Molecular ion H₂COHOCH₂⁺ in Model II forms in reactions



Analysis of chemical pathways shows that in both models the major reactions for CH₂OH and CH₃O formation on the grain surface are



with equal rates. It means that smaller binding energy of CH₃O affects its abundance (it becomes higher) and helps the CH₃O molecule replace CH₂OH in reactions described above. At the same time, in Model II the rate of reaction (3) is high enough to quickly destroy H₂CO. This is also the reason for high HCO abundance on the grain surfaces. One should note that the behaviors of HCO and CO maximum

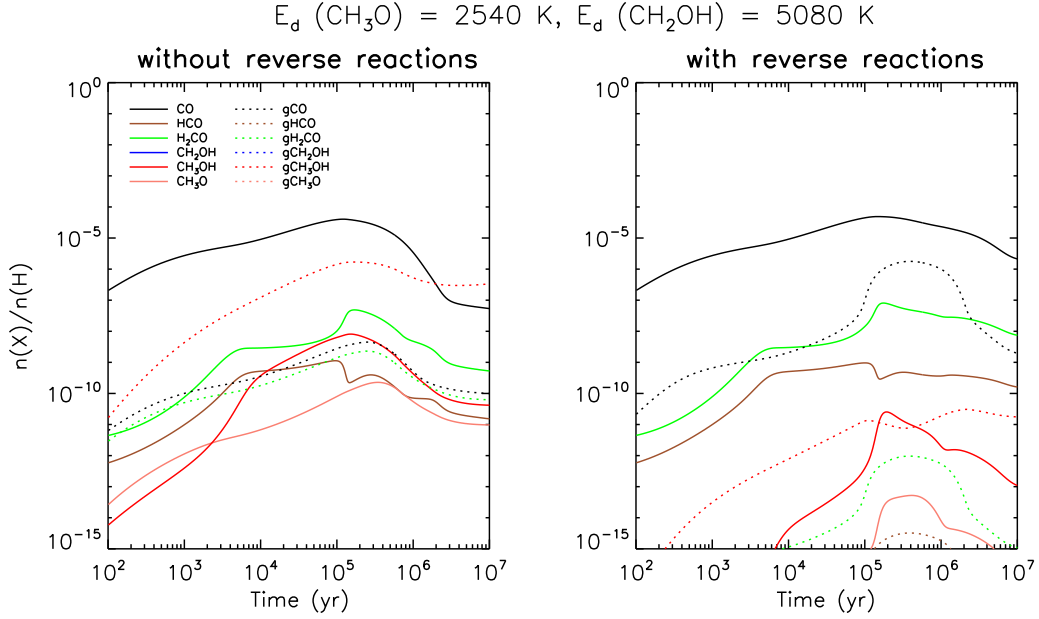


Fig. 1 Relative abundances of species versus time for the model of a cold dark cloud. These plots correspond to calculations with $E_d(\text{CH}_2\text{OH}) = 5080 \text{ K}$ and $E_d(\text{CH}_3\text{O}) = 2540 \text{ K}$. *Solid lines* represent molecules in gas phase, *dashed lines* – molecules on grain surfaces. The evolution time range is 10^2 – 10^6 yr.

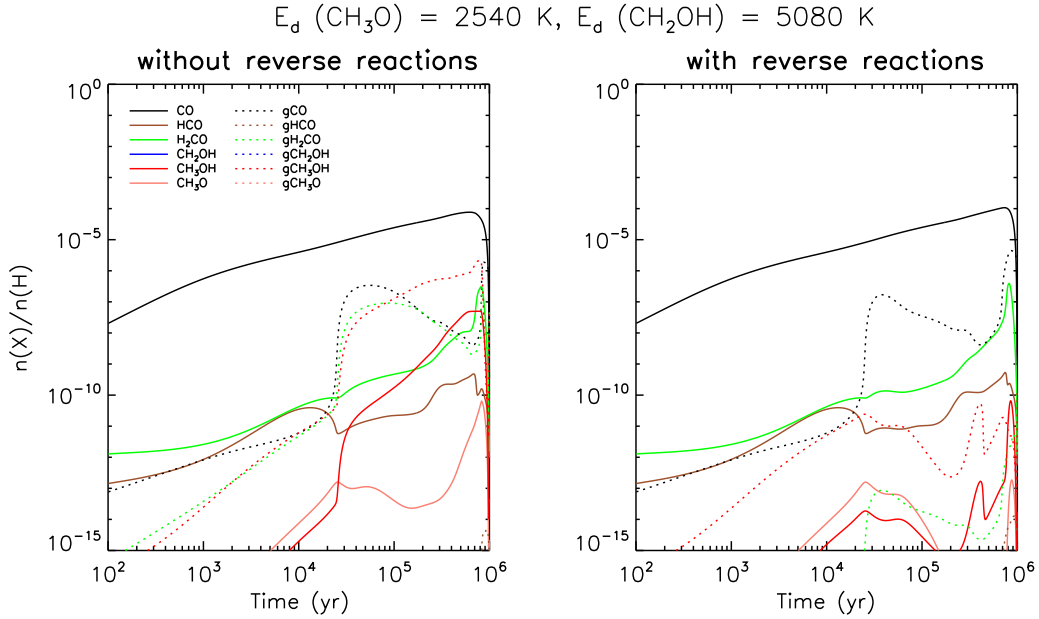


Fig. 2 Relative abundances of species versus time for the “cold” stage of the collapse model. These plots correspond to calculations with $E_d(\text{CH}_2\text{OH}) = 5080 \text{ K}$ and $E_d(\text{CH}_3\text{O}) = 2540 \text{ K}$. *Solid lines* represent molecules in gas phase, *dashed lines* – molecules on grain surfaces. The evolution time range is 10^2 – 10^6 yr.

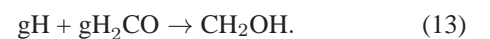
abundances on grain surfaces (see Fig. 1) are similar to each other and this can be also explained by the high rate of reaction (3).

Methanol on grain surfaces in both models is mainly formed by reactions



In the Model II efficiencies of reactions (11) and (12) decrease and accretion of CH_3OH from gas becomes important in chemical evolution of methanol on grain surfaces.

Gaseous CH_2OH in Model I can only be formed by the reaction



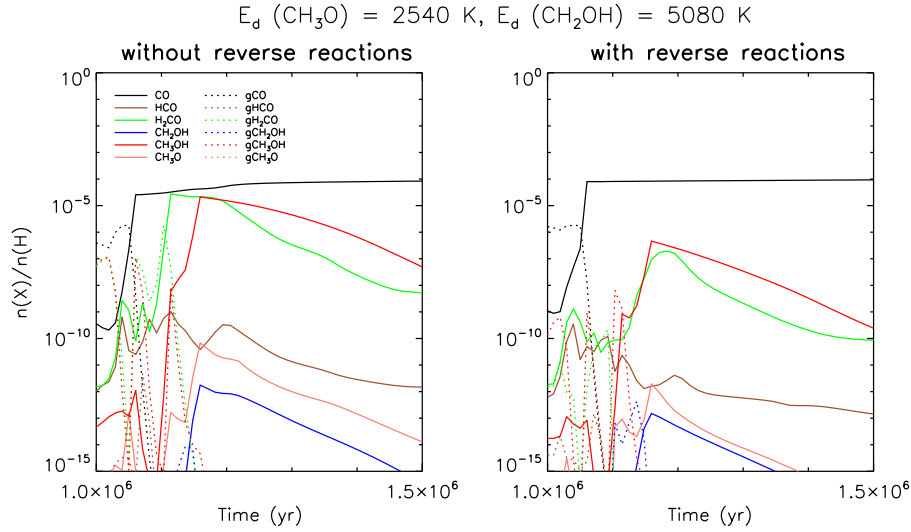


Fig. 3 Relative abundances of species versus time for the “warm-up” stage of the collapse model. These plots correspond to calculations with $E_d(\text{CH}_2\text{OH}) = 5080 \text{ K}$ and $E_d(\text{CH}_3\text{O}) = 2540 \text{ K}$. *Solid lines* represent molecules in gas phase, *dashed lines* – molecules on grain surfaces. The evolution time range is $1\text{--}1.5 \times 10^6 \text{ yr}$.

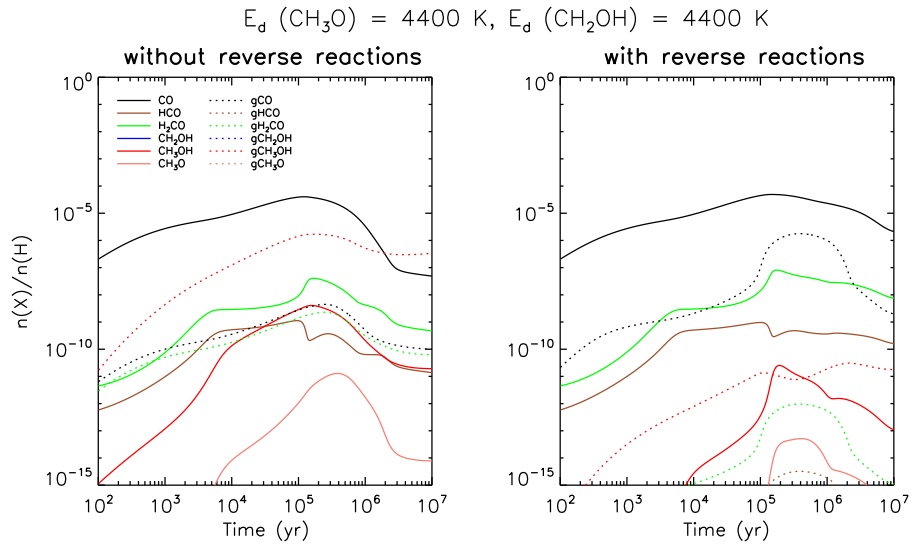
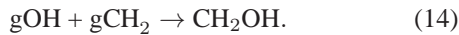
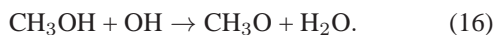


Fig. 4 Relative abundances of species versus time for the model of a cold dark cloud. These plots correspond to calculations with $E_d(\text{CH}_2\text{OH}) = E_d(\text{CH}_3\text{O}) = 4400 \text{ K}$. *Solid lines* represent molecules in gas phase, *dashed lines* – molecules on grain surfaces. The evolution time range is $10^2\text{--}10^6 \text{ yr}$.

The rate of this reaction in Model II decreases by a factor of five and the main route of CH_2OH formation in gas is



Gaseous CH_3O in Model I is formed in reactions



Reaction (16) becomes the most effective route for CH_3O formation and the rate of reaction (15) drops down to zero in Model II.

For CH_2OH and CH_3O , and then for CH_3OH , such changes in abundances and formation pathways can be

explained by decreasing H_2CO abundance on the grain surface as was mentioned above.

3.2 Collapse from the Translucent Cloud into the Dark Cloud

3.2.1 Cold stage

Abundances of molecules in the gas and on the grain surfaces for the first stage of the model of collapse are presented in Figure 2. Molecules with significant changes in abundances are the same as in the model of a cold dark cloud.

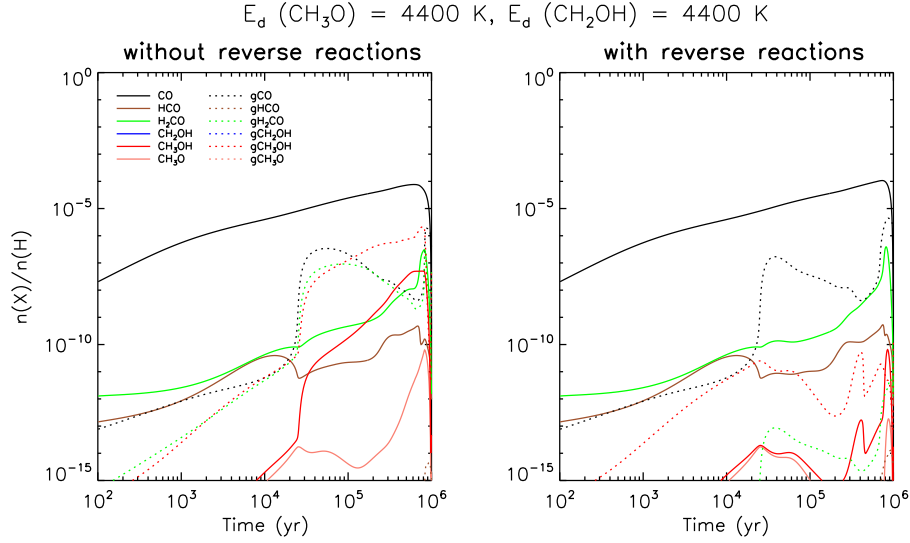


Fig. 5 Relative abundances of species versus time for the “cold” stage of the collapse model. These plots correspond to calculations with $E_d(\text{CH}_2\text{OH}) = E_d(\text{CH}_3\text{O}) = 4400 \text{ K}$. *Solid lines* represent molecules in gas phase, *dashed lines* – molecules on grain surfaces. The evolution time range is 10^2 – 10^6 yr.

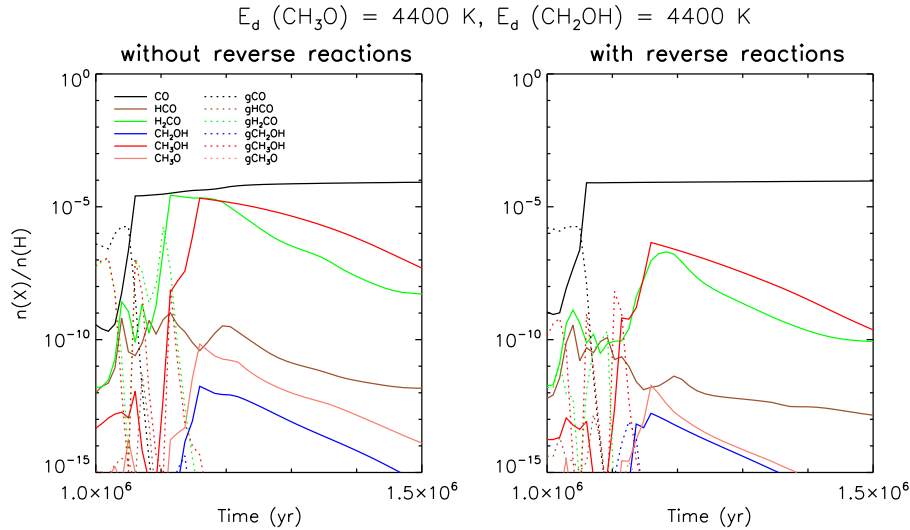


Fig. 6 Relative abundances of species versus time for the “warm-up” stage of the collapse model. These plots correspond to calculations with $E_d(\text{CH}_2\text{OH}) = E_d(\text{CH}_3\text{O}) = 4400 \text{ K}$. *Solid lines* represent molecules in gas phase, *dashed lines* – molecules on grain surfaces. The evolution time range is 1 – 1.5×10^6 yr.

In both types of models (Model I and II), gaseous methanol is formed in reactions (4) and (5) and released in gas phase by thermal desorption from the grain surfaces. The rate of reaction (9) is higher by a factor of two than in Model I. In Model I, the main pathways of CH_3O and CH_2OH formation are reactions (9) and (10), but in Model II almost all CH_3O molecules on grain surfaces are formed in the reaction



with temperatures of the medium at 18–20 K. At the same temperatures, CH_2OH is formed in the reaction



Then during the collapse, CH_3O begins to form in the reaction described by reaction (10), and CH_2OH forms in reactions (9) and (18).

As was described for the case of a cold dark cloud, the high rate of the reverse reaction (3) is responsible for decreasing H_2CO abundance on grain surfaces and it affects other reactions with this molecule.

3.2.2 Warm-up stage

Abundances of gaseous molecules and molecules on grains as a function of time for the second “warm” stage of the collapse are shown in Figure 3. Molecules with significant

changes in abundances are the same as in the case of the cold stage of the collapse. The warm-up stage is characterized by the square-law growing with temperature. Below we discuss molecular formation chains which occur at times when molecules start to approach their maximum values.

In both models (I and II), formation of CH_3O and CH_2OH becomes the object of our interest. Formation pathways of CH_3O (both gaseous and on the grain surfaces) are different from those described for the models of a cold dark cloud and cold stage of the collapse. Gaseous CH_3O in both models (I and II) is produced effectively in reactions (16) and (15), but reaction (15) is less effective than reaction (16). In Model I, CH_3OH forms in reactions (4) and (5) with equal efficiencies, but in Model II CH_3OH forms via the reaction (5) only. CH_2OH on the grain surfaces in Model I forms in reaction (9), but in Model II there are no efficient routes for its formation.

The main pathway of CH_3O formation on grains in both models is reaction (10) and the strongest reaction of its destruction is reaction (12). In Model II, reaction (10) becomes inefficient from chemical evolution of this molecule so CH_3O on the grain surfaces can be destroyed only in reaction (12), and there are no routes for its formation. All changes in chemical evolution of gCH_3O can be explained by the influence of the added reverse reactions. In Model II, one can see that H_2CO on grain surfaces is only destroyed in reaction (3), and there are no routes for effective CH_2OH or CH_3O formation on grain surfaces in contrast with Model I. This strongly affects formation of CH_3OH , because CH_2OH on the grain surfaces is a key reactant in reaction (5), and thus affects formation of gaseous CH_3O through reaction (16). Moreover, the rate of H_2CO destruction on grain surfaces in Model II is higher by a factor of two than its formation and this directly affects CH_3O formation in the reaction by reaction (10) on the grain surfaces.

In both models, CH_2OH in gas and on grain surfaces is formed less effectively than CH_3O . The main formation pathway of gaseous CH_2OH is reaction (14) and less effective reaction (13). In Model II, reaction (13) is inefficient in chemical evolution of gaseous CH_2OH , so only reaction (14) takes part in the formation of this molecule. Network analysis of CH_2OH formation on grain surfaces shows that in Model I destruction of CH_2OH on grain surfaces in reaction (11) proceeds more effectively than its formation in reaction (9). In Model II, reaction (9) disappears from chemical evolution, so CH_2OH on grains can be destroyed only in reaction (11). The most probable explanation is that CH_2OH chemical evolution is determined by faster destruction of H_2CO .

4 DISCUSSION AND CONCLUSIONS

In this study we analyzed the impact of added reverse reactions (reactions of H_2 abstraction) for HCO and H_2CO on the grain surfaces proposed by Minissale et al. (2016) for methanol chemistry. Analysis shows that the new reactions are highly efficient in the destruction of HCO and H_2CO and have a significant impact on abundances of molecules in the networks of methanol formation. In the models with reverse reactions, abundances of CH_3OH in gas phase and on grain surfaces decrease by 2–3 orders of magnitude.

These results are in somewhat mixed agreement with observations. In our model with added reverse reactions, fractional abundances of methanol are about 10^{-11} for the model of a cold dark cloud and 10^{-10} and 10^{-6} for the first and second stages of collapse correspondingly. Observed relative abundance of CH_3OH in the cold dark medium is about 2×10^{-9} (Irvine et al. 1991; Agúndez & Wakelam 2013; Jiménez-Serra, et al. 2016; Vasyunina et al. 2014) and in hot cores $10^{-7} - 10^{-5}$ (Bottinelli et al. 2007; Herbst & van Dishoeck 2009). This discrepancy raises questions about the exact values of activation barriers of reverse reactions for HCO and H_2CO on grain surfaces, which will be solved in future researches.

Moreover, it is important to study $\text{CH}_3\text{O}/\text{CH}_2\text{OH}$ evolution in the methanol formation chain. In the recent research of Wakelam et al. (2017), binding energies for CH_2OH and CH_3O are proposed to be $E_d(\text{CH}_2\text{OH}) = E_d(\text{CH}_3\text{O}) = 4400$ K. Figures 4, 5 and 6 display results of calculations for the model of a cold dark cloud and for both stages of the collapse from translucent into dark cloud with E_d values from Wakelam et al. (2017). Here we will name these cases Model Ia for the model without reverse reactions and new E_d values, and Model IIa for the model with reverse reactions and new E_d values. In the case of Model Ia, the most volatile molecules are CH_3O and CH_3OH . Such changes in CH_3OH abundances probably can be explained by decreasing of the reaction (4) rate.

In both stages of the collapse of the translucent cloud into a dark cloud, the only molecules for which abundances noticeably changed in both models (in comparison with Model I and II) are CH_2OH (both gaseous and on grains) and CH_3O in the gas phase. Analysis of its formation pathways shows that changes in binding energies of CH_2OH and CH_3O only affect efficiencies of reactions which were already described above. Therefore, the exact values of binding energies of CH_2OH and CH_3O do not affect the way of methanol formation.

Acknowledgements The reported study was funded by RFBR according to the research project 18-32-00645. The author thanks A. B. Ostrovskii and A. I. Vasyunin for

valuable discussions during the course of this work. The author thanks the anonymous referee for his helpful review of this paper.

References

- Agúndez M., & Wakelam V. 2013, *ChRv*, 113, 8710
- Baulch, D. L., Bowman, C. T., Cobos, C. J., et al. 2005, *Journal of Physical and Chemical Reference Data*, 34, 757
- Bottinelli, S., Ceccarelli, C., Williams, J. P., et al. 2007, *A&A*, 463, 601
- Fuchs, G. W., Cuppen, H. M., Ioppolo, S., et al. 2009, *A&A*, 505, 629
- Herbst, E., & van Dishoeck, E. F. 2009, *ARA&A*, 47, 427
- Irvine, W. M., Ohishi, M., & Kaifu, N. 1991, *Icarus*, 91, 2
- Jiménez-Serra I., et al. 2016, *ApJL*, 830, L6
- Kochina, O. V., Wiebe, D. S., Kalenskii, S. V., et al. 2013, *Astronomy Reports*, 57, 818
- Linnartz, H., Ioppolo, S., & Fedoseev, G. 2015, arXiv e-prints, arXiv:1507.02729
- McGuire, B. A. 2018, *ApJS*, 239, 17
- Minissale, M., Moudens, A., Baouche, S., Chaabouni, H., & Dulieu, F. 2016, *MNRAS*, 458, 2953
- Murga, M. S., Wiebe, D. S., Vasyunin, A. I., Varakin, V. N., & Stolyarov, A. V. 2020, *Russian Chemical Reviews*, 89, 430
- Öberg, K. I., Garrod, R. T., van Dishoeck, E. F., et al. 2009, *A&A*, 504, 891
- Rivilla, V. M., Beltr'an, M. T., Vasyunin, A., et al. 2019, *MNRAS*, 483, 806
- Tielens, A. G. G. M., Tokunaga, A. T., Geballe, T. R., et al. 1991, *ApJ*, 381, 181
- Vasyunin, A. I., Caselli, P., Dulieu, F., & Jiménez-Serra, I. 2017, *ApJ*, 842, 33
- Vasyunin, A. I., & Herbst, E. 2013, *ApJ*, 769, 34
- Vasyunin, A. I., & Herbst, E. 2013, *ApJ*, 762, 86
- Vasyunina T., et al. 2014, *ApJ*, 780, 85
- Wakelam, V., Loison, J.-C., Mereau, R., & Ruaud, M. 2017, *Molecular Astrophysics*, 6, 22
- Wakelam, V., & Herbst, E. 2008, *ApJ*, 680, 371
- Watanabe, N., & Kouchi, A. 2002, *ApJL*, 571, L173